Temporal and Spatial Ionospheric Variations of 20 April 2013 Earthquake in Yaan, China

Jun Tang, Yibin Yao, and Liang Zhang

***Abstract*—In this letter, we investigate the ionospheric variations associated with the Yaan earthquake that occurred on April 20, 2013 in China by using the total electron content (TEC) derived from ground-based Global Positioning System observations and a global ionosphere map (GIM). Geomagnetic and solar activities are taken into account. First, we focus on the coseismic ionospheric disturbances of the earthquake. The time period of the variations is about 15 min after the seismic rupture, and the maximum amplitude is about 0.1 TEC units. We then examine the preseismic ionospheric anomalies by the TEC values from the GIM and the electron density (Ne) values reconstructed by computerized ionospheric tomography. Temporal variations show that the TEC and Ne values simultaneously increased on April 5–8, 2013, which are 12–15 days before. This increase is possibly related to the earthquake. Spatial analysis shows that anomalies tend to appear around the epicenter and their conjugate points.**

***Index Terms*—Anomaly, ionosphere, ionospheric tomography, total electron content (TEC).**

I. Introduction

A GLOBAL Positioning System (GPS) provides an unprecedented capability of monitoring the ionosphere with the development of ionosphere remote sensing. This technique is widely used for detecting and investigating the ionospheric response to earthquakes. A large number of studies have been conducted on the coseismic ionospheric disturbances (CIDs) [1]–[8] and preseismic ionospheric anomalies associated with strong earthquakes [9]–[20]. For coseismic disturbances, Astafyeva *et al.* [2] analyzed the ionosphere response to the great Kurile earthquake in detail and found that the characteristics of CIDs depend on the distance from the epicenter. Liu *et al.* [8] reported the observed CIDs triggered by the shock-acoustic waves of the Chi-Chi earthquake. Cahyadi and Heki [4] studied the ionospheric disturbances associated with two large earthquakes and found that CIDs appeared 11–16 min after an earthquake and rapidly propagated northward (0.7 km/s). For preseismic anomalies, Liu *et al.* [13] employed the total electron content (TEC) derived from local ground-based GPS observations to study its variations during the Chi-Chi earthquake, and they found that the equatorial anomaly crest moved equatorward. In addition, the TEC value around the epicenter significantly decreased one, three, and four days before the earthquake. Liu *et al.* [14] also statistically investigated the variations of the ionospheric F2-layer critical frequency (foF2) during earthquakes with a magnitude (M) larger than 5.0 ($M > 5.0$) during 1994–1999 in the Taiwan area. The result showed that the foF2 decreased by more than 20% during the afternoon period, i.e., at 12:00–18:00 local time (LT), which significantly occurred within five days before the earthquakes. Researchers have used a global ionosphere map (GIM) to study the TEC anomalies before earthquakes worldwide, such as the 2004 Sumatra–Andaman earthquake [16], the 2008 Wenchuan earthquake [15], [21], the 2010 Haiti earthquake [17], the 2010 Chile earthquake [12], and the 2011 Tohoku–Oki earthquake [19], [22]. Their results showed that TEC anomalies appeared in time and space before an earthquake. Heki [10] used the Japanese dense network of GPS to detect the clear precursory positive anomaly of the ionospheric TEC around the focal region, and it was found that it started about 40 min before the 2011 Tohoku–Oki earthquake and reached nearly 10% of the background TEC. Only a statistical method was used to detect seismoionospheric precursors. In this letter, we research on coseismic and preseismic ionospheric variations, and we introduce a computerized ionospheric tomography (CIT) method to analyze ionospheric anomalies.

Numerous reports on earthquake-related ionospheric variations for some special earthquakes exist. These variations are usually associated with the forthcoming earthquake. Thus, in this letter, we examine the coseismic ionospheric variations of the GPS TEC derived from the measurement of ground-based GPS receivers. We then cross compare the GPS TEC extracted from a GIM and the electron density (Ne) reconstructed by CIT to analyze both the temporal and spatial seismoionospheric anomalous phenomena during the Yaan earthquake, which has a magnitude of 6.6 and occurred on April 20, 2013 in China.

II. Data and Methodology

An earthquake with a magnitude of 6.6 occurred in Yaan, China, at 00:02:47 universal time (UT) on April 20, 2013, with a depth of 14 km. The epicenter was located at 30.308 °N, 102.888 °E. The GPS raw data used in this letter come from the receivers of the Crustal Movement Observation Network of China (CMONOC) with a 30-s sampling rate [23]. Fig. 1 shows the epicenter selected GPS receivers. The GPS constellation transmits on two frequencies in the L-band, which are 1575.32 and 1227.60 MHz, respectively. The path integral of the

Manuscript received February 1, 2015; revised May 29, 2015 and July 18, 2015; accepted July 27, 2015. Date of publication August 18, 2015; date of current version October 27, 2015. This work was supported in part by the National Natural Science Foundation of China under Grant 41274022 and in part by the Key Laboratory of Geospace Environment and Geodesy, Ministry of Education under Grant 14-01-04.

J. Tang is with the School of Civil Engineering and Architecture, East China Jiaotong University, Nanchang 330013, China, and also with the Key Laboratory of Geospace Environment and Geodesy, Ministry of Education, Wuhan University, Wuhan 430079, China (e-mail: townjun@gmail.com).

Y. Yao and L. Zhang are with the School of Geodesy and Geomatics, Wuhan University, Wuhan 430079, China.

Color versions of one or more of the figures in this paper are available online at http://ieeexplore.ieee.org.

Digital Object Identifier 10.1109/LGRS.2015.2463081

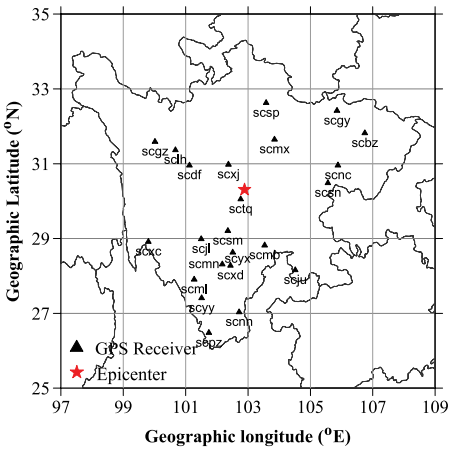

Fig. 1. Map of the epicenter of the 2012 Yaan earthquake, and the ground-based GPS receivers.

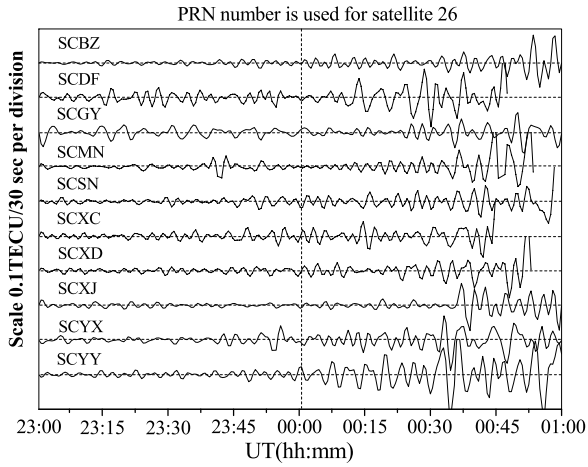

Fig. 2. VTEC along the ray path from the GPS receivers to satellite PRN 26 and the dTEC versus time. Each grid denotes 0.1 TECU/30 s (1 TECU $= 10^{16}$ electrons/m^2) on the vertical axis. The dashed line represents the time of the Yaan earthquake.

electron density along the satellite–receiver line of sight, which is commonly referred to as the slant TEC (STEC), can be calculated using the GPS phase measurements that are described in detail by Calais and Minster [24] and Leick [25]. The STEC between the satellite and a ground-based receiver can be written as

$$\text{STEC} = \left(\frac{1}{40.308}\right)\left[\frac{f_1^2 f_2^2}{(f_1^2 - f_2^2)}\right][(\lambda_1 L_1 - \lambda_2 L_2) + \text{const} + nL] \tag{1}$$

where L_1 and L_2 denote the carrier pseudoranges (in units of cycles) of the two frequencies f_1 and f_2, respectively, λ_1 and λ_2 are the corresponding wavelengths, const is the unknown initial phase ambiguity, and nL is the error in determining the phase path. The STEC is computed in TEC units (TECUs) where 1 TECU $= 10^{16}$ electrons/m^2. To detect temporal variations in the ionosphere, we calculate the ionospheric piercing point (IPP) of the line of sight, assuming a thin layer of the ionosphere at a 350-km altitude and the trace propagation of CIDs by a subionospheric point (SIP), which is a projection of an IPP to the Earth surface. From the given ionospheric height, the STEC along the ray path can be converted into the vertical TEC (VTEC) at its associated longitude and latitude usually using a simple cosine function of the satellite zenith. The accuracy of TEC estimates is related to the L_1 and L_2 accuracy. Effectively, because our interest is focused on high-frequency TEC perturbations, high-frequency variations have accuracy proportional to the accuracy of $\lambda_1 L_1 - \lambda_2 L_2$. We also employ differential TEC (dTEC) that is defined by subtracting each VTEC at $t = i + 1$ from its previous 30-s value at $t = i$, and we isolate the acoustic perturbations of interest by filtering the GPS raw TEC using a high-pass filter [5], [26]. We give an example of 30-s-sampling TEC data filtered with a passband between 4.3 and 5.8 MHz [27]. Accordingly, the amplitude and period of CIDs can be evaluated.

The GIM TEC data retrieved from the International Global Navigation Satellite System Service (IGS) are used to investigate the ionospheric variations before the Yaan earthquake and during background days. The global TEC covering ± 87.5 °N latitude and ± 180 °E longitude ranges with spatial resolutions of 2.5° and 5° every 2 h, respectively. To determine whether the TEC anomalies are really related to the earthquake, we need to take the geomagnetic and solar activity conditions during anomalous days into account. We also use the CIT technique to examine the anomalous variations in a 3-D electron density distribution. CIT, which is a new technique for understanding the ionosphere more fully, can reconstruct 3-D or 4-D structures of the ionosphere. Referring to CIT, the line integral of the electron density, i.e., the TEC, is measured over a large number of ray paths transitioning the ionosphere. This data set is inverted to produce an image of the electron density in ionosphere maps. In this letter, we reconstruct the electron density by CIT similar to the method of Nesterov and Kunitsyn [28].

III. Results on Ionospheric Variations Observed

A. Coseismic Disturbances

During the earthquake, eight GPS satellites passed around and over the Sichuan Province of China. However, we do the experiment by using these eight GPS satellites, and we find that only the TEC measurements of satellite PRN 26 are useful for our studies of the coseismic TEC perturbations above the focal regions of the earthquake and the CIDs forming. In Fig. 2, we show the temporal variations of the VTEC/30-s values and the time series from 23:00 UT to 01:00 UT recorded by satellite PRN 26 from some GPS receivers within Sichuan. The VTEC fluctuations have amplitudes of about 0.1 TECU. Compared with the quiet behavior before the earthquake, the sudden disturbances in the TEC are attributed to the CIDs triggered by the earthquake. About 15 min after the earthquake, the GPS stations registered a TEC perturbation with an amplitude of 0.06 TECU. At about 30 min, the amplitude of the waves reaches the maximum value of 0.1 TECU and then decreases to 0.02–0.04 TECU.

Fig. 3 shows the arrival times at different SIPs, and the distance from the center for these points' curves align on a certain line, which show a linear relationship between the travel times and the distances. The diagram for the records of satellite PRN 26 is also depicted. The nearest SIP was not disturbed until 28 min after the earthquake, and some further SIPs were always with a quiet behavior. When traveling away from the epicenter,

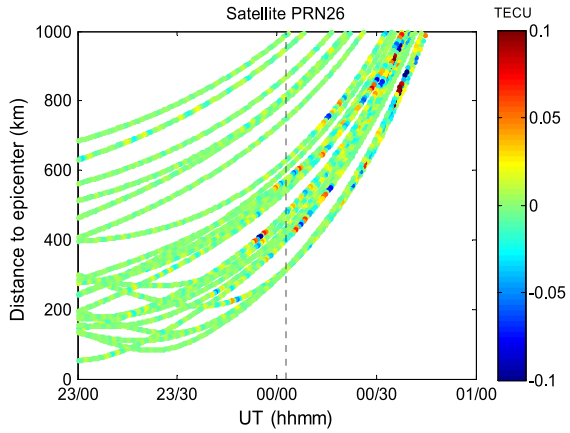

Fig. 3. Travel-time diagram of the CIDs calculated for satellite PRN 26 and all the GPS receiver time series. The epicentral distance is measured from the SIP to the epicenter. The dashed line represents the time of the Yaan earthquake.

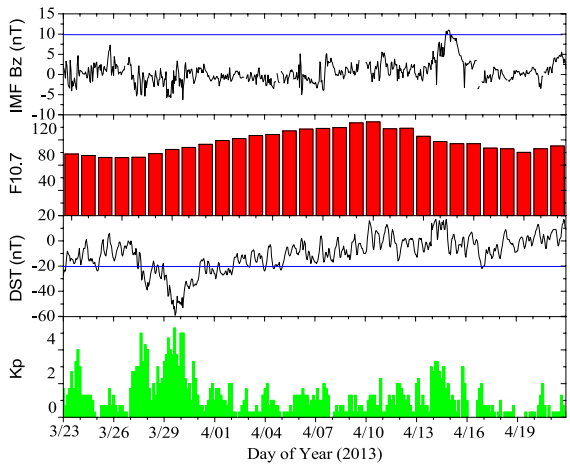

Fig. 4. Time series of the IMF Bz component, the F10.7 solar index, and the Dst and Kp geomagnetic indexes during the period from March 23, 2013 to April 21, 2013.

the associated CIDs slightly decrease and increase. At a time of about 35 min after the earthquake, the amplitude of the waves reaches the maximum value.

B. Preseismic Anomalies

1) GIM TEC: Solar and geomagnetic activities that are to have a strong impact on the ionosphere should be taken into account when analyzing ionospheric anomalies [17]. To check the possible effect of the solar and geomagnetic activities on the ionospheric behaviors, the z component of the interplanetary magnetic field (IMF) Bz, solar index F10.7, and geomagnetic indexes Dst and Kp are illustrated in Fig. 4. The IMF Bz component presented relatively large variations on April 14 and 15, but it is positive, which only has a small impact on the geomagnetic activity (negative Bz is much more geoactive). Sharp variations in Dst were on March 29 and 30, and for the Kp index, they were on March 23 and 27–30. Apart from the variations of the geomagnetic indexes, solar index F10.7 showed a moderate solar radiation. F10.7 indexes are relatively stable 15 days before the earthquake, which means that the solar activity is moderate overall. Therefore, in this figure, we can expect the effects of the solar and geomagnetic activities

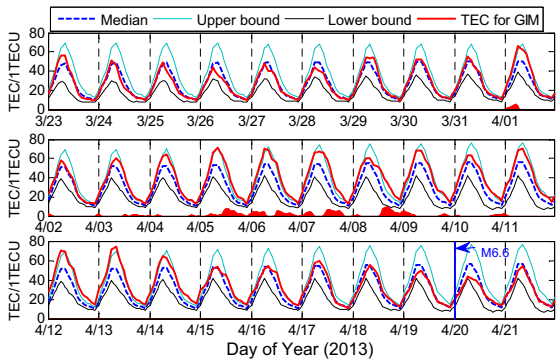

Fig. 5. Temporal distribution of the GIM TEC above the 2013 Yaan earthquake epicenter from March 23, 2013 to April 21, 2013. The red, blue, cyan, and black curves denote the GIM TEC, the associated median, and the median's UB and LB, respectively. The UB ($\mathrm{UB} = M + 1.5(\mathrm{UQ} - M)$) and the LB ($\mathrm{LB} = \mathrm{M} - 1.5(M - \mathrm{LQ})$) are used as references, where M, UQ, and LQ are the running median, the upper quartile, and the lower quartile on the previous 30 days, respectively. The red shaded areas are the differences between the observed TEC and the UB, which denote positive anomalies.

in the ionosphere TEC on March 23 and 27–30. We analyzed the causes of the ionospheric anomalies before the earthquake, and we attempted to exclude the anomalies that may have been caused by the solar and geomagnetic activities.

Fig. 5 illustrates the time series of the TEC above the epicenter during the Yaan earthquake. The TEC pronouncedly and significantly increased during the days of April 5–9 (11–15 days before the earthquake) without any decreasing anomaly. Considering the statistical analysis results in Ho *et al.* [12] and Liu *et al.* [14], we assume the duration of TEC anomalies longer than 8 h to be an anomalous day. At this time, we know that the solar and geomagnetic activities are quiet in Fig. 4, and we exclude the anomalies that may have been caused by solar and geomagnetic disturbances. Based on this criterion, the anomalous days associated with the earthquake can be found on April 5–8 (12–15 days before the earthquake). In fact, the epicentral TEC values at 12:00 UT (19:00 LT), 13:00 UT (20:00 LT), 12:00 UT (19:00 LT), and 16:00 UT (23:00 LT) on April 5–8 achieved their time point maximum values (increases) of positive deviation every day, respectively. At 16:00 UT (23:00 LT) on April 8, the time point maximum value (increases) of positive deviation was achieved among all these anomalous days before the Yaan earthquake. Therefore, the TEC over the epicenter not only statistically increases but also certainly increases during these time periods.

The ionospheric anomalies before the earthquake occurred not only above the epicenter but also in adjacent regions [16] or in the adjacent regions of the magnetic conjugate point. The affected possible coverage is expanded with the increase in the earthquake magnitude [29]. To illustrate the TEC variations at other latitude regions along the epicentral longitude and at other longitude regions along the epicentral latitude, we show the latitude–time–TEC map constructed by the 1–30 previous days' moving quartile along the longitude of 102.888 °E during the period of April 2–21, 2013 in Fig. 6. It can be seen that the significant anomalies in the TEC lasted approximately six days. The extreme enhancements at different times on April 5–8 mainly occurred in the regions around the epicenter and its magnetic conjugate point. In Fig. 6, the regions around the epicenter presented obvious anomalies on April 5–9. At the

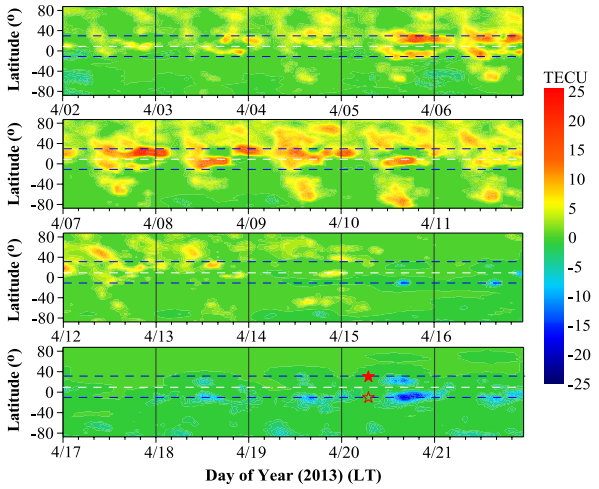

Fig. 6. Latitude–time–TEC plots are constructed by the 1–30 previous days' moving quartile along 102.888 °E on April 2–21, 2013 (LT). The solid and open start symbols are the epicenter and the corresponding conjugate point of the Yaan earthquake, respectively. The two blue dashed lines from top to bottom denote the location and the magnetic conjugate point of the epicenter, respectively, and the white dashed line is the magnetic equator.

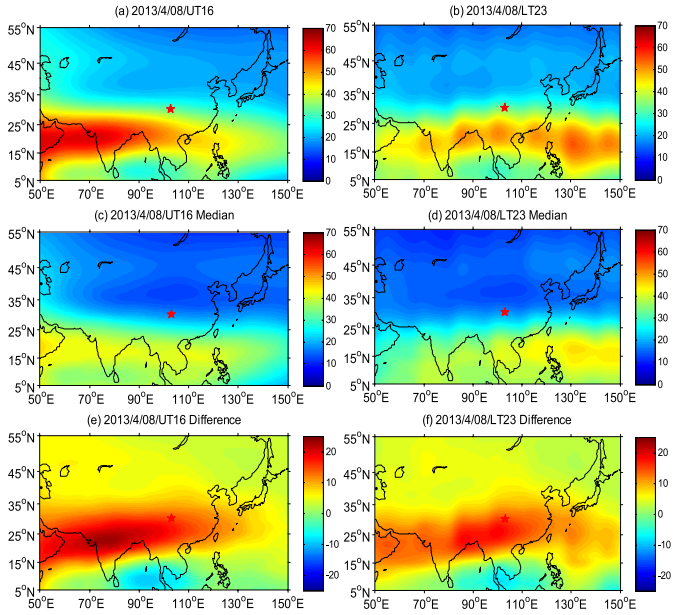

Fig. 7. TEC maps observed at 16:00 UT and the corresponding time 23:00 LT on day 12 before the Yaan earthquake. (a), (c), and (e) show the GIMs of the UT, and (b), (d), and (f) show the GIMs of the global fixed LT. (a) and (b) are the observed TEC, and (c) and (d) are the medians of the period of 1–30 days (from March 21, 2013 to April 19, 2013) before the earthquake. (e) and (f) denote the difference between the observed TEC and the associated median. Their units are TECU, and the asterisk is the epicenter of the Yaan earthquake.

same time, the magnetic conjugate point regions of the epicenter also presented clear anomalies on April 5–7, and the anomalies mostly occurred in the afternoon of April 5–9 (LT). For the Yaan earthquake under study, the epicenter was to the north of the northern crest of the equatorial ionization anomaly (EIA), and the EIA was shown to be intensified, resulting in an anomalous increase in the TEC at the locations of the epicenter. Was this an ionospheric precursor of the earthquake? The most possible cause for these preearthquake anomalies at low latitudes could be the strong vertical electric field bear in the earthquake preparation area. According to the formula of Dobrovolsky *et al.* [29] ($\rho = 10^{0.43M}$ km), the radius of this earthquake preparation zone would be ~700 km when $M = 6.6$. In fact, Fig. 5 clearly shows that the positive anomalies of the TEC are identified in a variation that is still within or slightly outside the upper bound (UB)–lower bound (LB) interval.

To further compare the TEC variations on April 5–8 and find their anomalies, the spatial distribution of the extreme enhancements within 30 days before the earthquake is analyzed. We calculate the difference of the TEC on a fixed day between the observed TEC and the associated median at fixed UT and LT. The relation between the UT and the LT is LT = UT + 7 at the epicenter area. Fig. 7 shows that the GPS TEC and the associated median yield remarkable reductions in the EIA. Taking into account the EIA or LT effects, a sequence of GIMs for a global fixed LT at 23:00 LT is also examined. It is found that the severe enhancements and the extreme maxima in the GPS TEC are once again mainly located around the forthcoming epicenter and EIA region (see Fig. 7). In Fig. 7, we have not considered the resolution error of the measurements and the systematic errors of the related products (GIMs). The anomaly area is larger in the longitude direction than in the latitude direction.

2) IED: To further understand the anomalies in the 3-D distributions of the ionospheric electron density (IED) above the epicenter, we use the CIT technique to calculate the difference between the reconstruction data at different times on April 5–8

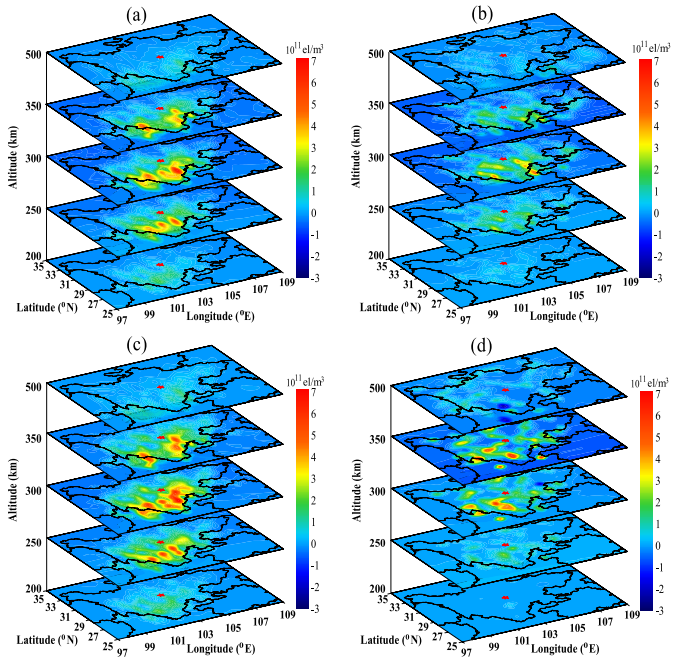

Fig. 8. IED slices at various altitudes. (a) At 12:00 UT on April 5. (b) At 13:00 UT on April 6. (c) At 12:00 UT on April 7. (d) At 16:00 UT on April 8. The solid symbol is the epicenter of the Yaan earthquake.

and its data that are constructed by the median value within 15 days before the earthquake. The inversion region is 25 °N–35 °N in latitude, 97 °E–109 °E in longitude, and 100–700 km in altitude. The spatial resolution is $0.5° \times 0.5° \times 50$ km along the longitude, the latitude, and the altitude. Fig. 8 shows the electron density for various altitude slices. The IED appears to have a noticeable enhancement in the regions over the epicenter

and even more toward the equator. These regions correspond to Fig. 7 derived from a GIM. A region where the IED variation in Fig. 8 coincides with the TEC variation in Fig. 7 on April 8 is also observed. Their anomalies generally are in the south of the epicenter. Meanwhile, the IEDs at altitudes of 250–350 km significantly increased around the epicenter. The IEDs at altitudes of 200 and 500 km increased slightly. The CIT analysis results are consistent with those of the GIM TEC analysis.

IV. Conclusion

To determine whether temporal and spatial ionospheric variations specifically appear during an earthquake, we examine CIDs and preseismic ionospheric anomalies. A CID is found in the Yaan earthquake. The smaller amplitudes can be explained by the dTEC. These CIDs start with positive anomalies, and the amplitudes of the negative anomalies reach the maximum value. We use GIM TEC data to study the preseismic ionospheric anomalies. To better understand ionospheric variations, we use a CIT technique to reconstruct a 3-D distribution of the IED around the epicenter. The results indicate that the ionospheric anomalies that occurred 12–15 days before the earthquake are likely to be preseismic ionospheric anomalies. At the same time, we find that an enhancement occurs not only in the adjacent regions of the epicenter but also in its magnetic conjugate point. This letter has provided a comprehensive study of the multiple aspects of temporal and spatial ionospheric variations. However, further investigation is required. We have not considered the resolution error of the measurements (the TEC) and the systematic errors of the related products (GIMs).

Acknowledgment

The authors would like to thank the International Global Navigation Satellite System Service (IGS) for the data used in this work and the Crustal Movement Observation Network of China (CMONOC) for the data provided by the GNSS Center, Wuhan University. The authors would also like to thank the anonymous reviewers for their valuable comments and suggestions.

References

[1] E. L. Afraimovich, N. P. Perevalova, A. V. Plotnikov, and A. M. Uralov, "The shock-acoustic waves generated by earthquakes," *Ann. Geophys.*, vol. 19, no. 4, pp. 395–409, Apr. 2001.

[2] E. Astafyeva, K. Heki, V. Kiryushkin, E. Afraimovich, and S. Shalimov, "Two-mode long-distance propagation of coseismic ionosphere disturbances," *J. Geophys. Res.*, vol. 114, no. A10, Oct. 2009, Art. ID. A10307.

[3] E. Astafyeva, S. Shalimov, E. Olshanshaya, and P. Lognonné, "Ionospheric response to earthquakes of different magnitudes: Larger quakes perturb the ionosphere stronger and longer," *Geophys. Res. Lett.*, vol. 40, no. 9, pp. 1675–1681, May 2013.

[4] M. N. Cahyadi and K. Heki, "Ionospheric disturbances of the 2007 Bengkulu and the 2005 Nias earthquakes, Sumatra, observed with a regional GPS network," *J. Geophys. Res.*, vol. 118, no. 4, pp. 1777–1787, Apr. 2013.

[5] R. Garcia, F. Crespon, V. Ducic, and P. Lognonné, "Three-dimensional ionospheric tomography of post-seismic perturbations produced by the Denali earthquake from GPS data," *Geophys. J. Int.*, vol. 163, no. 3, pp. 1049–1064, Dec. 2005.

[6] N. Imtiaz and R. Marchand, "Modeling of ionospheric magnetic field perturbations induced by earthquakes," *J. Geophys. Res.*, vol. 117, no. A04, Apr. 2012, Art. ID. A04320.

[7] V. E. Kunitsyn, I. A. Nesterov, and S. L. Shalimov, "Japan megathrust earthquake on March 11, 2011: GPS-TEC evidence for ionospheric disturbances," *JETP Lett.*, vol. 94, no. 8, pp. 616–620, Dec. 2011.

[8] J. Y. Liu *et al.*, "Coseismic ionospheric disturbances triggered by the Chi-Chi earthquake," *J. Geophys. Res.*, vol. 115, no. A8, 2010, Art. ID. A08303.

[9] E. Astafyeva and K. Heki, "Vertical TEC over seismically active region during low solar activity," *J. Atmos. Terr. Phys.*, vol. 73, no. 13, pp. 1643–1652, Aug. 2011.

[10] K. Heki, "Ionospheric electron enhancement preceding the 2011 Tohoku-Oki earthquake," *Geophys. Res. Lett.*, vol. 38, no. 17, pp. L17312–L17316, Sep. 2011.

[11] S. Hirooka, K. Hattori, M. Nishihashi, and T. Takeda, "Neural network based tomographic approach to detect earthquake-related ionospheric anomalies," *Nat. Hazards Earth Syst. Sci.*, vol. 11, pp. 2341–2353, Aug. 2011.

[12] Y. Y. Ho, H. K. Jhuang, Y. C. Su, and J. Y. Liu, "Seismo-ionospheric anomalies in total electron content of the GIM and electron density of DEMETER before the 27 February 2010 M8.8 Chile earthquake," *Adv. Space Res.*, vol. 51, no. 12, pp. 2309–2315, Jun. 2013.

[13] J. Y. Liu, Y. I. Chen, Y. J. Chuo, and H. F. Tsai, "Variations of ionospheric total electron content during the Chi-Chi earthquake," *Geophys. Res. Lett.*, vol. 28, no. 7, pp. 1383–1386, Apr. 2001.

[14] J. Y. Liu, Y. I. Chen, Y. J. Chuo, and C. S. Chen, "A statistical investigation of preearthquake ionospheric anomaly," *J. Geophys. Res.*, vol. 111, no. A05, May 2006, Art. ID. A05304.

[15] J. Y. Liu *et al.*, "Seimoionospheric GPS total electron content anomalies observed before the 12 May 2008 Mw7.9 Wenchuan earthquake," *J. Geophys. Res.*, vol. 114, no. A4, Apr. 2009, Art. ID. A04320.

[16] J. Y. Liu, Y. I. Chen, C. H. Chen, and K. Hattori, "Temporal and spatial precursors in the ionospheric Global Position System (GPS) total electron content observed before the 26 December 2004 M9.3 Sumatra-Andaman earthquake," *J. Geophys. Res.*, vol. 115, no. A9, Sep. 2010, Art. ID. A09312.

[17] J. Y. Liu *et al.*, "Observations and simulations of seismoionospheric GPS total electron content anomalies before the 12 January 2010 M7 Haiti earthquake," *J. Geophys. Res.*, vol. 116, no. A4, Apr. 2011, Art. ID. A04302.

[18] S. A. Pulinets and K. A. Boyarchuk, *Ionospheric Precursors of Earthquakes*. Berlin, Germany: Springer-Verlag, 2004.

[19] Y. Yao, P. Chen, H. Wu, S. Zhang, and W. Peng, "Analysis of ionospheric anomalies before the 2011 Mw9.0 Japan earthquake," *Chinese Sci. Bull.*, vol. 57, no. 5, pp. 500–510, Feb. 2012.

[20] F. Zhu, Y. Wu, Y. Zhou, and Y. Gao, "Temporal and spatial distribution of GPS-TEC anomalies prior to the strong earthquakes," *Astrophys. Space Sci.*, vol. 345, no. 2, pp. 239–246, Mar. 2013.

[21] B. Zhao *et al.*, "Is an unusual large enhancement of ionospheric electron density linked with the 2008 great Wenchuan earthquake?" *J. Geophys. Res.*, vol. 113, no. A11, pp. A11304, Nov. 2008.

[22] H. Le *et al.*, "The ionospheric anomalies prior to the M9.0 Tohoku-Oki earthquake," *J. Asian Earth Sci.*, vol. 62, pp. 476–484, Jan. 2013.

[23] Y. Yuan *et al.*, "Monitoring the ionosphere based on the Crustal Movement Observation Network of China," *Geod. Geodyn.*, vol. 6, no. 2, pp. 73–80, Mar. 2015.

[24] E. Calais and J. B. Minster, "GPS detection of ionospheric perturbations following the January 17, 1994, Northridge earthquake," *Geophys. Res. Lett.*, vol. 22, no. 9, pp. 1045–1048, May 1995.

[25] A. Leick, *GPS Satellite Surveying Third Edition*. Hoboken, NJ, USA: Wiley, 2004.

[26] J. Y. Liu, C. H. Lin, H. F. Tsai, and Y. A. Liou, "Ionospheric solar flare effects monitored by the ground-based GPS receivers: Theory and observation," *J. Geophys. Res.*, vol. 109, no. A1, Jan. 2004, Art. ID. A01307.

[27] P. Lognonné *et al.*, "Ground-based GPS imaging of ionospheric post-seismic signal," *Planet. Space Sci.*, vol. 54, no. 5, pp. 528–540, Apr. 2006.

[28] I. A. Nesterov and V. E. Kunitsyn, "GNSS radio tomography of the ionosphere: The problem with essentially incomplete data," *Adv. Space Res.*, vol. 47, no. 10, pp. 1789–1803, May 2011.

[29] I. P. Dobrovolsky, S. I. Zubkov, and V. I. Miachkin, "Estimation of the size of earthquake preparation zones," *Pure Appl. Geophys.*, vol. 117, no. 5, pp. 1025–1044, Jan. 1979.